AD-A161 686 HIGH VOLTAGE K SUB A -BAND GYROTRON EXPERIMENT(U) NAVAL RESEARCH LAB WASHINGTON DC S H GOLD ET AL. 20 NOV 85 NRL-MR-5602 1/1

UNCLASSIFIED F/G 20/7 NL

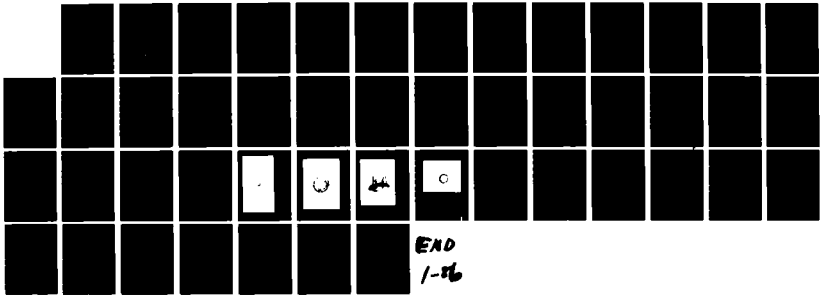

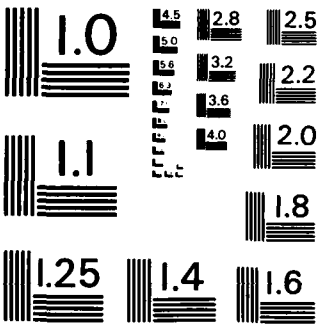

MICROCOPY RESOLUTION TEST CHART

NATIONAL BUREAU OF STANDARDS - 1963 - A

NRL Memorandum Report 5682

High Voltage K_a-Band Gyrotron Experiment

S. H. GOLD, A. W. FLIFLET, W. M. MANHEIMER,
W. M. BLACK, V. L. GRANATSTEIN,* A. K. KINKEAD,
D. L. HARDESTY AND M. SUCY†

High Power Electromagnetic Radiation Branch
Plasma Physics Division

**University of Maryland*
College Park, MD 20742

†*JAYCOR, Inc.*
Alexandria, VA 22304

November 20, 1985

This work was supported by the Office of Naval Research, the Defense Nuclear Agency under Subtask X99QMXVF, work unit 00007 and work unit title "Gyrotron Development," and also by the Department of Energy in a cooperative program with the Lawrence Livermore National Laboratory.

NAVAL RESEARCH LABORATORY
Washington, D.C.

SECURITY CLASSIFICATION OF THIS PAGE

REPORT DOCUMENTATION PAGE

AD-A161 686

1a REPORT SECURITY CLASSIFICATION UNCLASSIFIED	1b RESTRICTIVE MARKINGS
2a SECURITY CLASSIFICATION AUTHORITY	3 DISTRIBUTION/AVAILABILITY OF REPORT Approved for public release; distribution unlimited.
2b DECLASSIFICATION/DOWNGRADING SCHEDULE	
4 PERFORMING ORGANIZATION REPORT NUMBER(S) NRL Memorandum Report 5682	5 MONITORING ORGANIZATION REPORT NUMBER(S)
6a NAME OF PERFORMING ORGANIZATION Naval Research Laboratory	6b OFFICE SYMBOL (If applicable) Code 4740
6c ADDRESS (City, State, and ZIP Code) Washington, DC 20375-5000	7a NAME OF MONITORING ORGANIZATION
8a NAME OF FUNDING/SPONSORING ORGANIZATION ONR, DNA and DOE	8b OFFICE SYMBOL (If applicable)
8c ADDRESS (City, State, and ZIP Code) Arlington, VA 22217 Washington, DC 20585 Washington, DC 20305	7b ADDRESS (City, State, and ZIP Code)
	9 PROCUREMENT INSTRUMENT IDENTIFICATION NUMBER
	10 SOURCE OF FUNDING NUMBERS

PROGRAM ELEMENT NO	PROJECT NO	TASK NO.	WORK UNIT ACCESSION NO.
(See page ii)			

11 TITLE (Include Security Classification)
High Voltage K_a-Band Gyrotron Experiment

12 PERSONAL AUTHOR(S) Gold, S.H., Fliflet, A.W., Manheimer, W.M., Black, W.M., Granatstein, V.L.,* Kinkead, A.K., Hardesty, D.L., and Sucy, M.†

13a TYPE OF REPORT	13b TIME COVERED	14 DATE OF REPORT (Year, Month, Day)	15 PAGE COUNT
Interim	FROM 1/84 TO 3/85	1985 November 20	48

16 SUPPLEMENTARY NOTATION *University of Maryland, College Park, MD 20742
†JAYCOR, Inc., Alexandria, VA 22304 (Continues)

17 COSATI CODES		
FIELD	GROUP	SUB-GROUP

18 SUBJECT TERMS (Continue on reverse if necessary and identify by block number)
High voltage, Gyrotron, Intense, K_a-band, Experiment, Beam, Febetron

19 ABSTRACT (Continue on reverse if necessary and identify by block number)

A new high voltage, intense beam K_a-band gyrotron experiment is underway, using a 350-400 keV, 0.5-1 kA beam from a short-pulse Febetron pulser. High power operation at 35 GHz has been observed, with 20 MW (±3 dB) produced at ~8.5% efficiency in a "whispering-gallery" TE_{62} mode. Operation in other modes, and at other frequencies has also been studied.

20 DISTRIBUTION/AVAILABILITY OF ABSTRACT	21 ABSTRACT SECURITY CLASSIFICATION
☒ UNCLASSIFIED/UNLIMITED ☐ SAME AS RPT ☐ DTIC USERS	UNCLASSIFIED

22a NAME OF RESPONSIBLE INDIVIDUAL	22b TELEPHONE (Include Area Code)	22c. OFFICE SYMBOL
S. H. Gold	(202) 767-3292	Code 4740

DD FORM 1473, 84 MAR 83 APR edition may be used until exhausted
All other editions are obsolete

SECURITY CLASSIFICATION OF THIS PAGE

10. SOURCE OF FUNDING NUMBERS

PROGRAM ELEMENT NO.	PROJECT NO.	TASK NO.	WORK UNIT ACCESSION NO.
61153N	RR011-09-41		DN880-061
62715H	DE-AI03-84SF12188		DN480-686

16. SUPPLEMENTARY NOTATION (Continued)

This work was supported by the Office of Naval Research, the Defense Nuclear Agency under Subtask X99QMXVF, work unit 00007 and work unit title "Gyrotron Development," and also by the Department of Energy in a cooperative program with the Lawrence Livermore National Laboratory.

CONTENTS

I. INTRODUCTION 1

II. EXPERIMENTAL SETUP 3

III. EXPERIMENTAL RESULTS 6

IV. THEORY 15

V. DISCUSSION 19

ACKNOWLEDGMENTS 21

REFERENCES 34

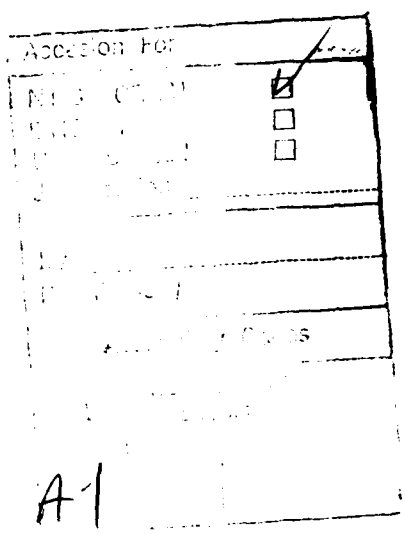

HIGH VOLTAGE K_a-BAND GYROTRON EXPERIMENT

I. Introduction

The Cyclotron Resonance Maser (CRM) is under development as a versatile millimeter-wave radiation source capable of high peak and average power and high efficiency. To date the highest powers and efficiencies have been achieved by CRM oscillators having the "gyrotron" configuration. In this device, an electron beam with high transverse momentum and propagating in a strong applied magnetic field interacts with a waveguide mode which is close to cutoff. Coherent radiation is generated near the cyclotron frequency or one of its harmonics. Research on gyrotrons was recently reviewed by Flyagin et al. [1].

Many of the earliest cyclotron maser experiments were carried out at high currents and voltages (kA's at $\gtrsim$1 MeV) employing short-duration pulses ($\lesssim$100 nsec) provided by pulseline accelerators using plasma-induced field emission (cold) cathodes. These devices typically used beams with low values of the pitch ratio $\alpha \equiv v_\perp/v_\parallel$, which is a measure of the free energy available to the interaction, and with large spreads in velocity and energy. The devices were usually operated in a superradiant mode, or lacked well-defined cavity structures. Such devices produced impressive powers (often >>100 MW), but typically at relatively low efficiencies. For example, Granatstein and coworkers obtained X-band microwave power as high as 1 GW using a 3.3 MeV, 80 kA electron beam [2]. On the other hand, recent millimeter-wave gyrotron oscillator development has emphasized high average power devices based on thermionic diode technology and using well-defined microwave cavity

Manuscript approved August 12, 1985.

structures. Such devices have produced several hundred kilowatt powers and high efficiencies (over 50%) using high quality, moderate voltage ($\lesssim$100 keV) electron beams with currents of $\lesssim$50 A [3]. Of particular note is a 60 GHz gyrotron which has produced 200 kW of cw power at an efficiency of 40% [4].

Future applications of millimeter-wave radiation, such as advanced rf accelerators and high power radars, may require sources with very high peak powers and efficiencies, which will tend to push gyrotrons to higher voltage operation. For this reason, it is of interest to return to cyclotron maser experiments on pulseline accelerators in order to investigate the peak power potential of true cavity gyrotrons based on relativistic (0.25-1 MeV), multi-kA electron beams.

Cold cathode gyrotron experiments have achieved high powers and efficiencies at conventional microwave frequencies. For instance, Ginzburg et al. [5] reported 25 MW at 20% efficiency in an experiment at 10 GHz and Didenko et al. [6] reported ~500 MW at 30% efficiency at 3 GHz. In a recent experiment, Voronkov et al. [7] extended this work to millimeter wavelengths, reporting the production of 23 MW at 40 GHz with 5% efficiency using a 350 kV, 1.3 kA electron beam produced by a cold cathode diode. That experiment operated in a TE_{13} cavity mode and employed an axially-bifurcated cavity for mode stabilization. A novel diode was used to form a relatively high quality, high α (~0.84) electron beam. This is of particular interest since beam formation is a critical issue for cold cathode gyrotrons operating at millimeter wavelengths.

Theory and scaling calculations suggest that much higher powers and efficiences should be achievable in relativistic gyrotron oscillators

operating at millimeter wavelengths. Improved efficiencies would require optimization of the cavity design and the beam parameters. Extension to still higher powers should be possible by increases in the beam current and voltage. In this paper, we report on the initial operation of a new high-voltage K_a-band gyrotron experiment that is designed to explore these issues. This experiment employs a 600 kV, 6 kA short-pulse Febetron pulser to permit investigation of electron beam formation and gyrotron operation at higher voltages than the previous work. We plan to extend operation to the more highly overmoded gyrotron cavities necessary for higher power operation. In this context, we plan to explore the problems of mode stability in such cavities for a variety of modes. For instance, whispering-gallery modes have superior mode competition properties, and may be stable for high-power single-mode operation without the addition of mode selective structures, such as the axial slots used to stabilize TE_{1n} modes in the earlier work. We also plan to investigate efficiency enhancement through cavity and axial field tapering.

In the initial experiments, a 350-400 keV, 0.5-2 kA electron beam was used to produce peak powers of up to ~20 MW at 35 GHz in a TE_{62} mode with an estimated efficiency of 8.5%. Stable operation in the TE_{62} and other whispering-gallery modes has been obtained in a conventional cylindrical gyrotron cavity; this is in contrast to the TE_{1n} gyrotron studied by Voronkov et al. [7] which utilized a more complicated cavity geometry to achieve mode stability.

II. Experimental Setup

In this work we are investigating gyrotron operation in K_a-band, principally in the vicinity of 35 GHz, using an electron beam from a

600 kV, 6 kA, 55 nsec compact Febetron pulser. Figure 1 illustrates the experimental geometry. A cold cathode diode configuration based on the approach of Voronkov et al. [7] is used. The absence of a thermionic cathode permits experimental operation at the "diffusion-pump" pressures typical of high voltage, pulsed power experiments, i.e. $\sim 10^{-5}$ Torr, rather than at the ultra-high vacuums necessary in conventional gyrotron devices. This permits use of oil-coated high-voltage insulators and plastic output windows, and generally facilitates rapid changes in the experimental setup. In the present experiments, operation is typically at 350-400 kV. A thin annular beam (0.5-2 kA) is launched from the edge of a 3.8-cm-diam disk-shaped carbon cathode in a foilless diode configuration. Initially, as pointed out by Voronkov et al. [7], the tranverse velocity is of order $v_\perp \lesssim |\vec{E}\times\vec{B}|/B^2$, where $\vec{E}$ is the electric field near the cathode and is primarily radial with a magnitude of $\sim$1 MV/cm. $\vec{B}$ is an axial magnetic field of order 10 kG which provides magnetic insulation for the diode. Thus, initially, $\beta_\perp = v_\perp/c \lesssim 0.3$. Due to the edge geometry, a large velocity spread is expected. This qualitative behavior is confirmed by electron trajectory calculations using the Herrmannsfeldt code [8]. The transverse velocity then is increased by non-adiabatic effects and by magnetic compression as the beam is transported through a tapered drift tube to an overmoded gyrotron cavity with a radius of 1.60 cm. This tapered region is lined with lossy material to inhibit the buildup of spurious modes. The electron beam flow and transverse velocity are controlled by a pair of pulsed solenoidal magnets, one producing a "trim" magnetic field of $\sim$10 kG at the cathode and the second producing up to 25 kG at the cavity. A soft iron ring is positioned enclosing the electron beam just

downstream from the trim magnet windings to sharpen the magnetic transition from the diode region to the region dominated by the fringing magnetic fields of the main field solenoid. The precise effect on the beam of this configuration is difficult to model, but is estimated to give a final $\alpha \sim 0.5\text{-}1$ with considerable spread.

Through variation of the cathode diameter and of the ratio of the magnetic field at the cathode to the field in the gyrotron cavity, the beam is positioned on a selected radial rf-field maximum of a desired cavity mode. (The radius of the beam is accurately determined by photographing the beam-induced fluorescence of a 6-μm sheet of aluminized mylar that is stretched across the beam upstream from the cavity.) An appropriate value of magnetic field is chosen at the cavity to provide gain at the resonant frequency of the cavity in the desired mode. After passage through the gyrotron cavity, the electron beam expands in the decreasing axial magnetic field of the main magnet, and is collected on the wall of the output waveguide. The output window is placed sufficiently far downstream to avoid contact with the electron beam.

In these experiments, the cavity was designed to be resonant near 35 GHz in several possible operating modes, including the $TE_{10,1}$ and TE_{62} modes. The input end of the cavity has a tapered section for efficiency enhancement by contouring the axial profile of the rf field [9]. The tapered wall begins below cutoff of the desired mode. The output end of the cavity is defined by a change in cavity wall slope. The microwave emission passes through a tapered output coupler to the final 14-cm diameter of the output waveguide leading to a polyethylene vacuum window. The frequencies of the lowest order $TE_{mn\ell}$ (ℓ=1) modes in

the vicinity of 35 GHz are shown in Fig. 2. The length of the cavity corresponds to approximately 10 cyclotron orbits for a 350 kV electron beam with $\alpha \sim 0.75$ and the cavity Q-factor, neglecting ohmic and mode conversion effects, is Q=520 [10]. This interaction length and Q-factor are longer and higher, respectively, than the values corresponding to optimum efficiency and power [11], and were chosen conservatively to allow cavity startup with electron beam currents as low as 100-200 Amps and $\alpha \sim 0.5$. The cavity was made from thin stainless steel to allow rapid penetration of the pulsed magnetic field, and was coated with a thin layer of gold to reduce ohmic losses.

III. Experimental Results

The initial tests of the new experimental configuration were designed to characterize and optimize the beam formation process. Studies were carried out using witness plates, beam masks, fluorescent screens [12], and a Faraday cup. A variety of cathode diameters, lengths and materials were employed, and the beam properties studied as a function of the magnetic field values at the cathode and at the gyrotron cavity. In each case, a thin annular beam is formed and subsequently compressed as the magnetic field increases from the cathode to the gyrotron cavity. The character of the beam trajectories was studied by forming small beamlets, via a beam mask with four ~0.5 mm radial slots that was positioned in the vicinity of the cathode, and studying the beamlet cross sections in the region of the cavity. This allows an examination of the beam transverse velocity distribution [13]. Each beamlet smears into a larger pattern via phase-mixing of the

Larmor orbits due to electron parallel velocity spread. Ideally, the mask is positioned before significant phase-mixing of the Larmor orbits occurs, so that each slit samples only a single phase of the Larmor orbits of electrons originating at the cathode. In this case, the downstream pattern is generated by electrons in each beamlet with a single guiding center, and the measurement of the beamlet structure via fluorescent screen measurements can be unfolded into a direct measure of the distribution function of beam Larmor radius (r_L), and hence, transverse velocity $v_\perp = \Omega r_L$, where Ω is the relativistic cyclotron frequency. The fluorescent screen measurement produced filled-in circles, unlike the ring-like patterns seen by Bogdanov et al. [13] This may have been caused by the presence of greater transverse velocity spread in our experiment, or by phase-mixing of Larmor orbits upstream from the mask. Our measurements are consistent with a large spread in $v_\perp$, and a maximum value of $\alpha \sim 1$.

A process of optimization of the beam parameters was carried out consistent with the basic geometry of the diode, drift tube, and cavity. Following this, a set of microwave generation experiments was carried out to investigate the experimental gyrotron capabilities with the optimized beam parameters obtainable without major modifications in the beam generation system. These microwave studies were carried out both with standard microwave waveguide (WR-28) components, and via a low pressure cell in which the photographic observation of microwave-induced gas breakdown could be used as an experimental diagnostic of the microwave mode pattern.

The microwave system (see Fig. 3) consisted of a single detection channel that led from a small microwave pickup (typically located

adjacent to the 14-cm-diam polyethylene output window of the experiment) to a calibrated crystal detector, through ~11 m of WR-28 waveguide, a 20 dB directional coupler (to reduce the detected signal), a calibrated rotary-vane attenuator, a K_a-band band-pass filter, and a narrowband step-twist filter [14] that could be used to select varying bandwidths about a center frequency of 35 GHz. The waveguide pickup was surrounded by microwave absorber to avoid substantial reflections back into the experiment. The experimental pickup was typically just the open end of a section of K_a-band (WR-28) waveguide. This pickup could be translated across the output window using a clamp riding on a section of triangular optical bench, and could be rotated via a waveguide twist to sample either the radial or azimuthal components of the mode as a function of position across the horizontal diameter of the output window.

The Febetron output voltage waveform has a ~55 nsec "flat-top" with a slow ~15% voltage ripple. For the proper choice of parameters, the microwave signal will persist for up to ~50 nsec in spite of this voltage variation, demonstrating the bandwidth of the gyrotron interaction in a short cavity. More typically, as the main and trim magnetic fields are varied, the microwave emission will consist of one or more 10-20 nsec spikes.

Figure 4 shows an experimental mode pattern, in both radial and azimuthal polarizations, produced at an operating voltage of 350 kV with a 700 A electron beam and a magnetic field of 18.8 kG. The beam radius was ~1.16 cm and the average pitch ratio α of the beam was estimated to be ~0.75. The microwave signal is measured in mW at the crystal detector at a fixed level of total attenuation, as a function of position across the left horizontal radius of the experimental output

window. (The azimuthal symmetry of the emission will be addressed later in this paper.) Due to the problem of experimental reproducibility, at least three experimental discharges were measured in each polarization at each radial position, and Fig. 4 plots the mean and its standard deviation for this data. The observed mode pattern is clearly hollow and has a well-defined radial structure in each polarization. The mode pattern can be compared to the predicted gyrotron cavity modes that should be resonant in the vicinity of 35 GHz. (See Fig. 2.) The 1.6 GHz FWHM of the step-twist filter setting used for these measurements would discriminate against the TE_{33} mode at 34 GHz. (Sample measurements with the filter FWHM set as low as 500 MHz, which would strongly discriminate against the TE_{33} mode, demonstrated that TE_{33} radiation was unimportant for these experimental parameters.) While there is little similarity between the experimental observations and either the TE_{14} or $TE_{10,1}$ modes shown in Fig. 5, the match with the TE_{62} radial mode structure is strong, although the relative amplitudes of the various radial peaks in each polarization do not agree perfectly with those predicted for this mode. This observed deviation from the expected TE_{62} mode pattern is believed to be due in part to mode conversion in the output coupler, whose walls expand outward at an angle of 10° from the diameter of the gyrotron cavity to the i.d. of the output waveguide that leads to the end of the experimental vacuum enclosure. Subsequent analysis of the mode conversion process in the output coupler suggests that up to 50% conversion into other TE_{6n} modes could be expected through the length of this taper, principally into the TE_{63} and TE_{61} modes. Such a superposition of modes at the output window could well explain the deviation of Fig. 4 from the predictions for the TE_{62} mode.

High power gyrotron devices typically operate in high order cavity modes, whose identification is important for the understanding of the device operation. For this purpose, a breakdown diagnostic was constructed consisting of a low pressure cell, capable of either side-on or end-on observation. This cell could either attach directly to the output window of the experiment, or be coupled to the experimental output window via a microwave lens which would serve to collimate the microwave emission. The low-pressure cell could be used to directly observe the output mode as a breakdown pattern across the face of its upstream window. This was accomplished by varying the pressure in the cell until a clear breakdown pattern could be observed on the face of this window. At appropriate pressures, typically in the range of 10 to 60 Torr, the breakdown would then clearly delineate the position of electric field maxima across the output window produced by a particular mode in the output waveguide of the experiment.

The original expectation for this diagnostic was the observation of clear concentric rings due to the generation of rotating cavity modes in the gyrotron cavity. The pattern of these rings across a radius could then be compared directly to radial field predictions for various cavity modes. Since the radial and azimuthal electric fields are temporally 90° out of phase in any specific waveguide mode, it would be expected that the breakdown image would display separate rings for the radial maxima of both the radial and azimuthal electric fields. Such concentric rings were generally easily observed, as seen in Fig. 6, which is for the same parameters as the microwave measurements shown previously. (Note that in order to preserve the concentric ring

structure easily visible on the original photograph, it was necessary for publication to reproduce Fig. 6 at a much higher contrast than that of the original image. This has tended to enhance the appearance of azimuthal asymmetry well beyond that suggested by the original image.) Fig. 6 displays principal breakdown rings at approximately 3.5, 4.5, and 5.5 cm, in reasonable agreement with the microwave measurements of Fig. 4. However, in many other cases, such as the case illustrated in Fig. 7, which is for the same cavity magnetic field, but with a ~10% larger beam radius, a periodic azimuthal structure could also be observed in the breakdown image. (Such a pattern would tend to complicate the results of a radial scan of the microwave emission such as shown in Fig. 4; however, Fig. 6 shows little sign of such azimuthal periodicity.) This standing structure allowed a direct determination of the azimuthal index of the radiation simply by counting azimuthal maxima and dividing the result by two. This feature was particularly valuable since, as mentioned previously, calculations suggest that the 10° taper in the cavity output coupler, that connects the 1.60 cm cavity diameter to the 14 cm diameter of the output waveguide, was capable of generating up to 50% mode conversion from the original operating mode of the gyrotron cavity. Such mode conversion would be expected to change the radial structure of gyrotron cavity mode by transferring energy to modes of different radial indices, and therefore interfere with the recognition of the radial structure of the original mode in the pattern observed with the microwave pickup. However, since the output coupler is azimuthally symmetric, it would be expected to preserve the azimuthal mode index. Combining the measured azimuthal index with the predictions of the mode map (Fig. 2) and the resonant frequency of the experiment

allowed an unambiguous identification of the operating mode in the cavity. In future experiments, a 5% output taper will be used which should cause a substantially reduced level of mode conversion.

The azimuthal standing structure could also be observed in side-on photographs as shown in Fig. 8. These side-on photographs were taken using a microwave lens to collimate the microwave emission from the output window, and with a metal reflector further downstream to create an axial standing structure in the breakdown cell, due to the interference of emitted and reflected microwave radiation. The result is the production of a pattern of breakdown streamers at the azimuthal maxima of the mode, in this case a TE_{62} mode, that once again allows a simple determination of the azimuthal mode number. The axial standing structure occurs at half-wavelength intervals, and could in principle be used to determine the gyrotron operating frequency. However, for 35-GHz operation, the frequency is already known to sufficient accuracy via the waveguide step-twist filter.

The implication of a standing azimuthal breakdown structure is that the interaction is coupling to both positive and negative azimuthal indices of the specific operating mode (i.e., to circularly-polarized modes with both right-hand and left-hand polarization), since the coherent superposition of the two is required to produce an azimuthal standing mode. The general clarity of the azimuthal structure in the breakdown image is most likely a function of the ratio of power in each of the counterrotating modes. The presence of both counter-rotating modes may be due in part to finite beam thickness or to slight decentering of the beam in the gyrotron cavity, since the radial dependence of the coupling coefficient is different for each mode.

Using the breakdown technique, simultaneous coupling to both the $TE_{\pm 10,n}$ and $TE_{\pm 6n}$ modes could be observed on single shots, for which the cavity magnetic field was resonant near 35 GHz. Such a case is shown in Fig. 7, which reveals an azimuthal index of 10 on the outer edge of the breakdown image, and an azimuthal index of 6 towards the center. (Whether the two modes were in fact simultaneous, or were sequential within the single voltage pulse, is not presently determined.) This observation is consistent with the mode map (Fig. 2) that shows the nominal resonant cavity frequencies of the $TE_{10,1,1}$ mode to be 35.24 and the TE_{621} mode to be 35.13. By reducing the beam diameter by ~10% by increasing the ratio of main field to trim field, the $TE_{10,1}$ mode pattern could be suppressed, leaving only the TE_{62} mode visible in the breakdown pattern of Fig. 6. Operating with the magnetic field detuned from 35 GHz operation, still other modes could be identified via their azimuthal standing-wave signatures combined with their resonant magnetic fields. By selecting a 24.2 kG magnetic field, a mode with an azimuthal index of 9 was generated (Fig. 9), which we identified by its resonant magnetic field as a TE_{92} mode occurring in the vicinity of 45.8 GHz.

The difficulty in fabricating a sensitive single-pulse calorimeter to detect the high-order modes present in this experiment has thus far prevented a direct measurement of the single-shot microwave energy. Instead, since the entire detection system, with the exception of the coupling to the WR-28 microwave pickup, was absolutely calibrated, it is possible to estimate the total microwave power in the experiment by integrating the detected power in both radial and azimuthal polarizations over the face of the output window. To do this, we assume that the emission is locally (on the scale length of the waveguide

pickup) very similar to a plane wave, and assume that all the energy striking the waveguide aperture in the correct polarization is coupled into the waveguide. (We did not calibrate the coupling coefficient through the waveguide aperture, but we believe that the assumption of 100% coupling will somewhat underestimate the true power.) In addition, we assume that the power distribution is azimuthally symmetric. (Sample measurements at the radial maxima of $|E_r|^2$ and $|E_\theta|^2$ along the four horizontal and vertical radii demonstrated substantial [±2 dB] asymmetries, but in each case the left horizontal radius plotted in Fig. 4 was found to be within 1 dB of the mean value for the four radii.) We account for the following factors: waveguide loss at 35 GHz between the experiment and the screen room; the fractional coupling in a directional coupler; the setting on an in-line calibrated attenuator; and the insertion loss of the waveguide filters. Power measurements are then performed with a K_a-band crystal detector. Each of the passive components was calibrated at 35 GHz by substitution against a calibrated rotary-vane attenuator, and the crystal detector was absolutely calibrated at 35 GHz against a thermistor power meter over the entire range of detected signals, so that it was not necessary to assume detector linearity.

Averaging the detected microwave signal shown in Fig. 4 over the measured mode pattern via the assumption of azimuthal symmetry, we find an average signal of ~1.3 mW in both radial and azimuthal polarizations. Adding these together (3 dB) and increasing this value by the ratio of the waveguide aperture to the area of the output window (28 dB as a power ratio) to sum over the output window, and by calibrated waveguide loss (12 dB), directional coupler loss (20 dB),

attenuator setting (38 dB), and filter insertion loss (1 dB), produces an estimated emitted power of 20 MW. Given the problem of azimuthal asymmetries, the concern for the precise coupling coefficient into the waveguide aperture, and the problem of small calibration errors for each of the microwave components, we estimate that the overall error of this measuring process is ±3 dB. The data in Figs. 4 and 6 suggest that this power is produced principally in a TE_{62} mode, but no assumption to this effect has been used in the power determination.

IV. Theory

The theory of gyrotrons with relativistic beams is similar to that of gyrotrons with weakly relativistic beams, and has been reviewed by Bratman et al. [15]. In gyrotrons, the optimum efficiency scales as $\eta \sim [N_c(1-\gamma_o^{-1})]^{-1}$, where γ_o is the relativistic factor and N_c is the number of cyclotron orbits occurring in the cavity. Thus, to obtain efficient high voltage operation, the interaction length should be short. Peak efficiency occurs for $N_c \sim 5\text{-}10$, compared to the optimum of $N_c \sim 15\text{-}30$ for a 70 keV beam. This leads to a wider interaction bandwidth at higher voltage, and the increased probability of mode competition in overmoded cavities.

Estimates of efficiency and starting currents for TE modes with resonant frequencies near 35 GHz were obtained by integrating the equations of motion for an electron in a prescribed cavity field and averaging over the phase of the electron entering the cavity. The output power was found from the power balance relation $P_\omega = \omega W/Q$, where ω is the wave frequency (rad/sec), W is the cavity stored energy, and Q

is the cold cavity Q-factor. The corresponding beam power P_B was found by applying the power balance relation $P_\omega = \eta P_B$, where η is the efficiency. A tractable set of equations based on a previously developed slow-time-scale formulation was used. For this application the equations derived in [16] for the interaction with a single TE mode have been generalized to include the interaction with the rf magnetic field components. The axial profile of the cavity rf field and the cavity Q-factor and resonant frequencies were calculated for the cavity shown in Fig. 1 using weakly irregular waveguide theory as discussed in [10]. The present calculations do not include electron beam velocity spread, self-field effects, or electron beam loading effects on the cavity rf fields. The latter effects, for weakly relativistic gyrotrons, have been considered by Lau [17] for an axicentered electron beam in a cylindrical waveguide, and by Fliflet et al. [16] for low Q gyromonotrons. Lau's results indicate that the beam loading effect on the transverse structure of the rf fields is small. Fliflet et al. showed that electron beam loading affects the axial profile of the rf fields, and thus the loaded Q and operating frequency of gyrotron oscillators, but that the minimum starting current and maximum efficiency are not significantly changed. However, these conclusions may need to be modified for the present high current regime, and are under investigation.

The present calculations consider the interaction of the electron beam with a circularly-polarized rf mode of the form

$$\vec{E} = \mathrm{Re}\left\{\vec{e}\,(r,\vartheta,z)\; f(z)\; e^{i(\omega t - m\theta)}\right\} \qquad (1)$$

where ω is the wave frequency, $\vec{e}(r,\theta,z)$ is a transverse vector mode function [16], and $f(z)$ is the axial profile function. The sign of m determines the direction of rotation. For positive m, the dc beam current required to sustain a given electric field magnitude in the cavity will be inversely proportional to the square of the normalized electron beam-rf mode coupling coefficient for a TE_{mn} mode, which is given by

$$C^{+} = \frac{1}{\left[\pi(1 - m^2/x_{mn}^2\right]^{1/2} J_m(x_{mn})} \quad \frac{J_{m-s}(k_{mn}R_o)}{R_w} \qquad (2)$$

where J_m is a regular Bessel function, s is the harmonic number, x_{mn} is the nth zero of $dJ_m(x)/dx$, R_o is the electron orbit guiding center radius, R_w is the cavity wall radius, and $k_{mn}=x_{mn}/R_w$ is the tranverse wave number. For negative m, the coupling coefficient (C^-) is given by Eq. (2) with m replaced by $|m|$ and $J_{m-s}(k_{mn}R_o)$ replaced by $(-1)^s J_{m+s}(k_{mn}R_o)$. The values of the squares of the coupling coefficients, which is a measure of the strength of the coupling of the electron beam to the rf electric fields, are shown for the $TE_{\pm 6,2}$ and $TE_{\pm 10,1}$ modes in Fig. 10. The solid curves correspond to positive m and the dashed to negative m. The experimental electron beam radius obtained by optimizing the experimental parameters with respect to output power at 35 GHz is also shown in Fig. 10. This position is evidently close to optimum for coupling to the circularly-polarized TE_{-62} mode, whose rotation direction is opposite to that of the electron orbits.

The threshold currents for oscillation ("starting currents") were calculated for the $TE_{\pm 6,2}$, $TE_{\pm 10,1}$, $TE_{\pm 1,4}$ and $TE_{\pm 3,3}$ modes by considering the limit

$$I_{th} = \lim_{E_o \to 0} \frac{P_\omega(E_o)}{V_o \eta(E_o)} ,$$

where E_o is the maximum cavity electric field amplitude and V_o is the beam voltage. As shown in Fig. 2, the resonant frequencies of the first three transverse modes are within a few hundred MHz of 35 GHz and would be transmitted by the narrowband filter used in the experiment. The last mode resonates at 34.0 Ghz, but due to the wide bandwidth of the interaction ($\Delta\omega/\omega \sim N_c^{-1} \sim 0.1$), is a possible competing mode. Starting currents for the $TE_{-6,2}$, $TE_{10,1}$ and $TE_{-3,3}$ modes for the experimentally observed e-beam radius of 1.16 cm are shown in Fig. 11. The minimum starting currents for the TE_{14} modes are found to be much larger (>1kA) at this e-beam position. Fig. 11 shows, as expected from Fig. 10, that the $TE_{-6,2}$ mode has the lowest starting current (~50A) and is therefore most likely to be excited. This is consistent with the data obtained in the experiment. As the e-beam radius is increased, the starting current of the $TE_{10,1}$ mode decreases and the excitation of this mode becomes more probable, again in agreement with the gas breakdown measurements.

The calculated electronic efficiency and output power for the $TE_{-6,2}$ mode as a function of electron beam current, optimized with respect to magnetic field, are shown in Fig. 12. The calculations use the experimentally determined electron beam energy of 350 keV and assume $\alpha = 0.75$. The measured value of α has a large uncertainly but the data indicates that $\langle\alpha\rangle \lesssim 1$ and that there is a large spread in this ratio. We note that even a large velocity spread is not expected to greatly

reduce the gyrotron efficiency. With the above parameters the maximum efficiency (~17%) for the present cavity occurs at approximately 250 Amps. For the operating current of ~700 A, the calculated efficiency is 11% which is in good agreement with the experimental value of ~8.5%.

The power obtainable from high voltage gyrotrons is ultimately limited by space-charge depression of the electron beam voltage. However, we find this effect to be small for the present operating parameters, since the estimated voltage drop due to beam space-charge is approximately 20 kV, implying a 2.5% change in γ_o.

V. Discussion

The present experimental configuration has succeeded in generating an estimated 20 MW at an electronic efficiency of 8.5% in the vicinity of 35 GHz, using a ~350 keV, ~700 A beam from a compact Febetron pulser. Operation has been observed in the TE_{-62} mode, although the mode purity of the output radiation appears somewhat degraded. For some beam radii, coupling to the $TE_{+6,2}$ was also evident. Additional coupling to the $TE_{\pm 10,1}$ modes was also observed near 35 GHz for large beam radii, and other cavity modes were generated at other frequencies when the axial magnetic field at the cavity was detuned from 35 GHz operation.

Although further investigation is needed, the present data suggests that the use of whispering-gallery modes will permit efficient single-mode operation in relativistic gyrotrons using overmoded cavities without the use of transverse mode-selective structures such as the

slotted or bifurcated cavities used to stabilize TE_{1n} modes. This has certain advantages such as higher intrinsic efficiency and simplified gyrotron design. As expected, the observed operating mode is the one with the lowest starting current.

The principal limiting factor in the present experiment is believed to be the electron beam used in the interaction. Limitations on the original diode design have not permitted us to produce a 600 kV, 2 kA beam with $\alpha \sim 1$ as originally intended, and experimentally we are limited to somewhat lower values of each of these parameters. With the intended beam parameters, output powers in the 100-200 MW range are expected [11]. Based on our calculations, the observed experimental operation (~20 MW) is consistent with that which would be expected for the present beam parameters (350 kV, 0.7 kA, $\alpha \sim 0.75$), and large improvements in the power and efficiency cannot be achieved without improvements in the beam. For this reason, an improved beam formation system has been designed, and will be tested in the near future. In this new scheme, initial beam formation will be separated from the addition of transverse kinetic energy. Transverse energy will be provided either through resonant pumping via a transverse wiggler magnetic field, or by passage through a nonadiabatic step in magnetic field. We are also investigating the use of a beam formation technique involving the adiabatic compression of a beam produced from a MIG-like gun designed for operation at high voltage.[18] With the production of a suitable beam, the gyrotron cavity will be redesigned and the cavity Q-factor lowered to permit higher power operation, since the present cavity was designed principally for low starting current operation consistent with our present derated beam parameters.

References

Acknowledgments

We are grateful for the technical assistance provided by H. Alberts and R. Lee, and for informative discussions with Dr. M.E. Read. This work was supported in part by the Office of Naval Research, in part by the Defense Nuclear Agency, and in part by the Department of Energy in a cooperative program with the Lawrence Livermore National Laboratory.

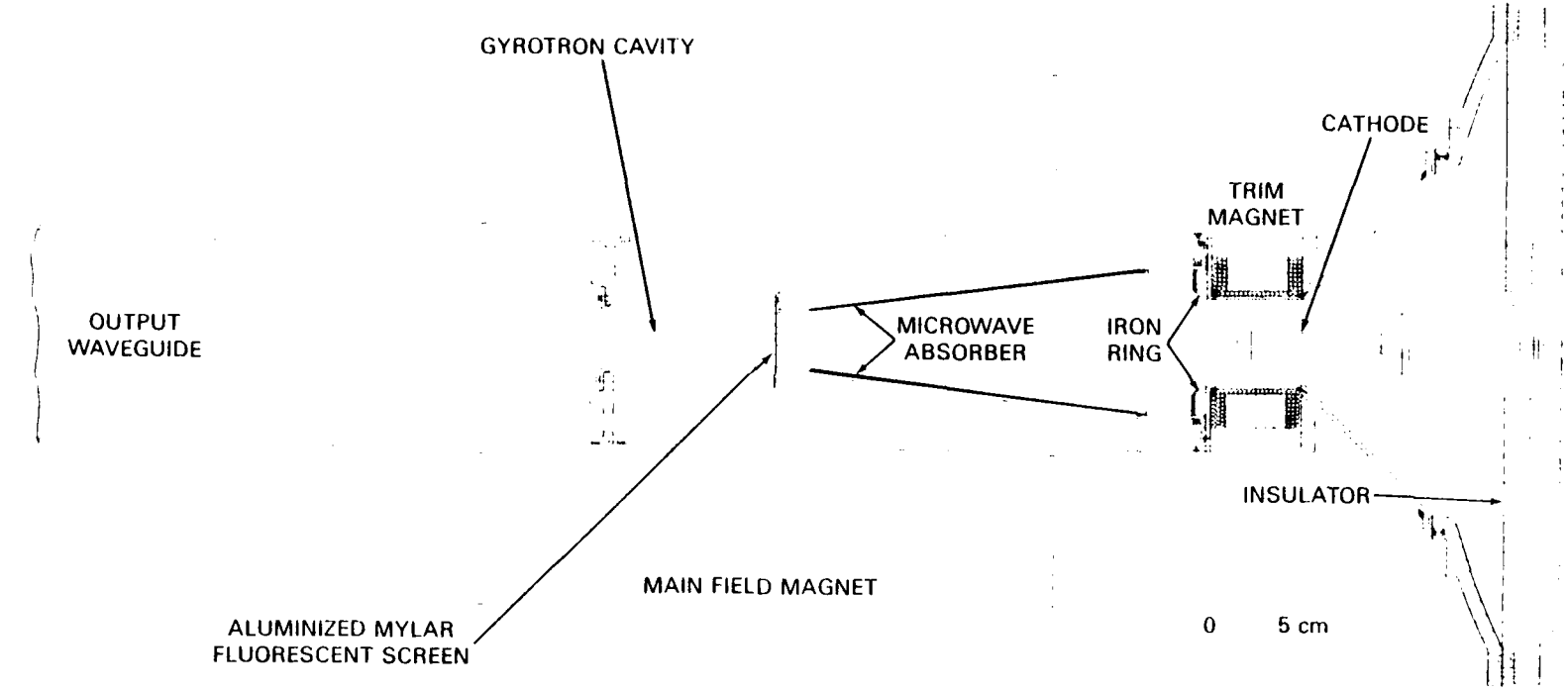

Fig. 1. Experimental setup for the intense-beam gyrotron experiments.

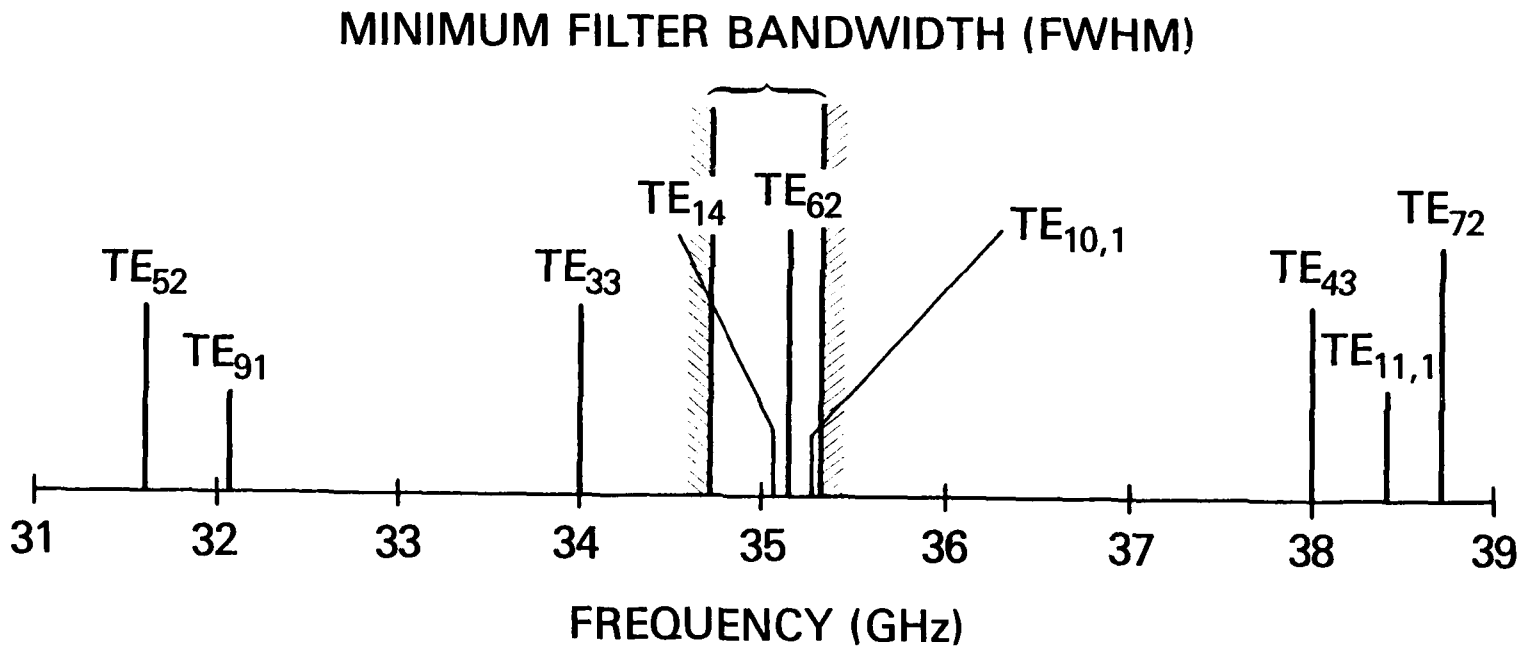

Fig. 2. Map of the gyrotron ℓ=1 cavity modes between 31 and 39 GHz.

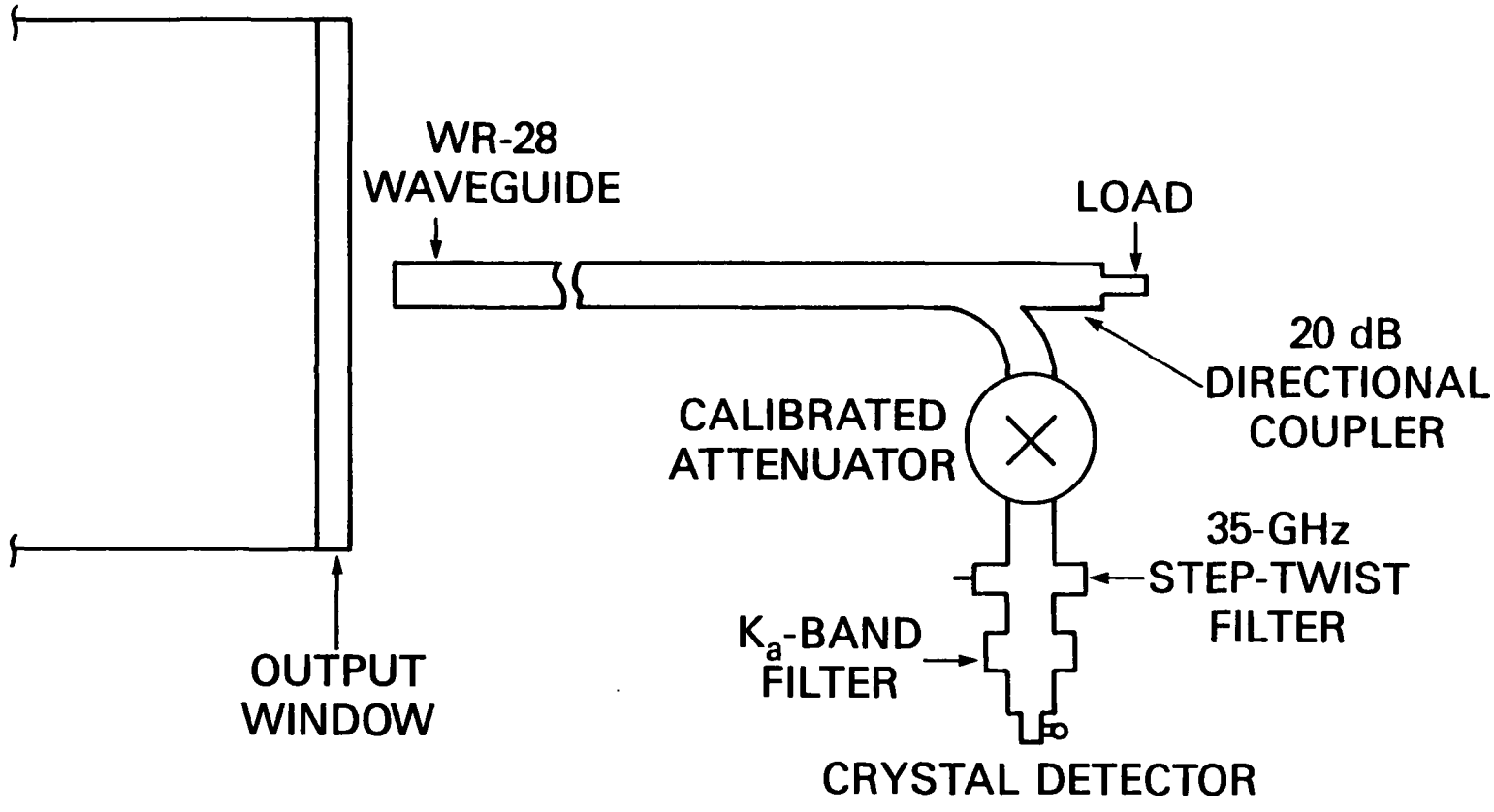

Fig. 3. Schematic diagram of the microwave diagostics.

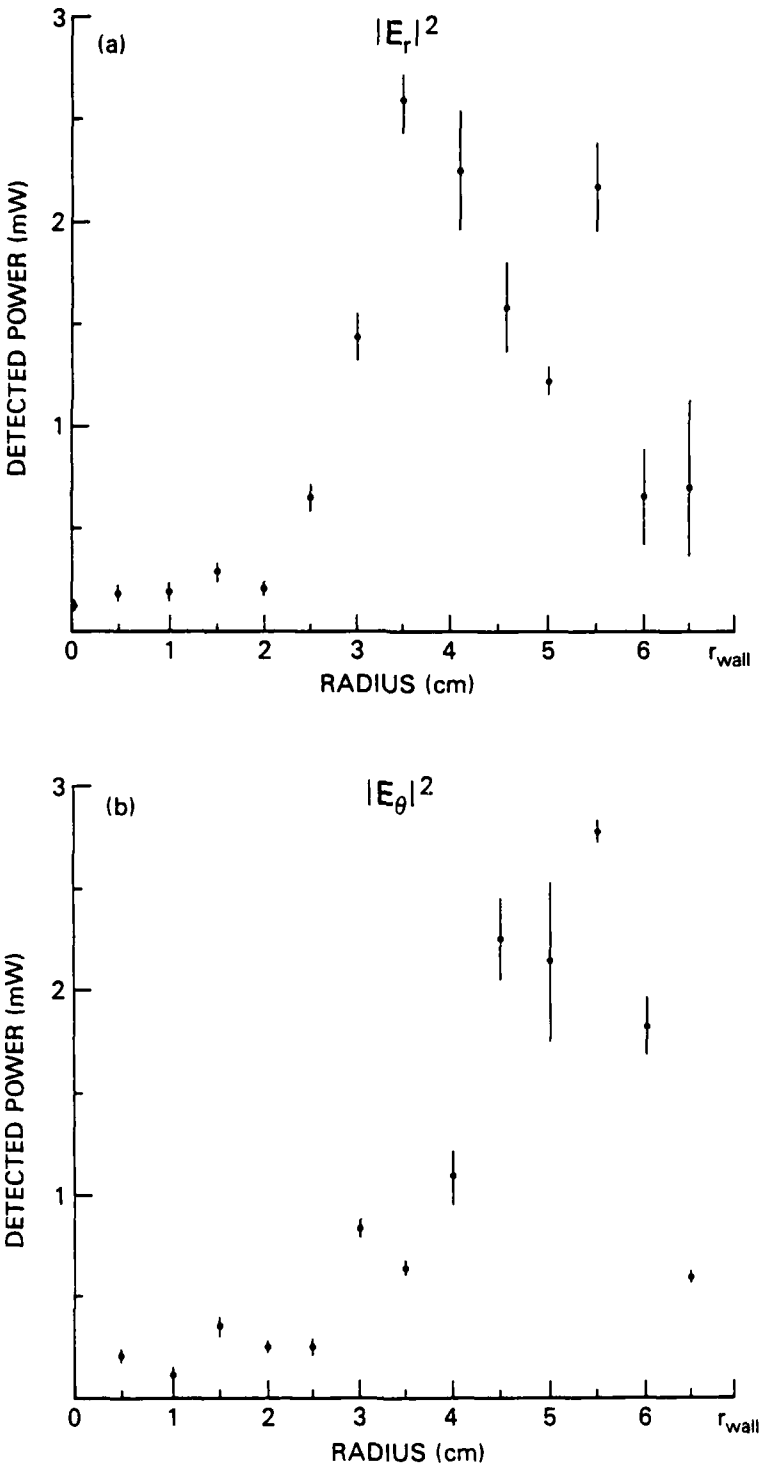

Fig. 4. Detected power as a function of radius across the experimental output window for (a) $|E_r|^2$ and (b) $|E_\theta|^2$.

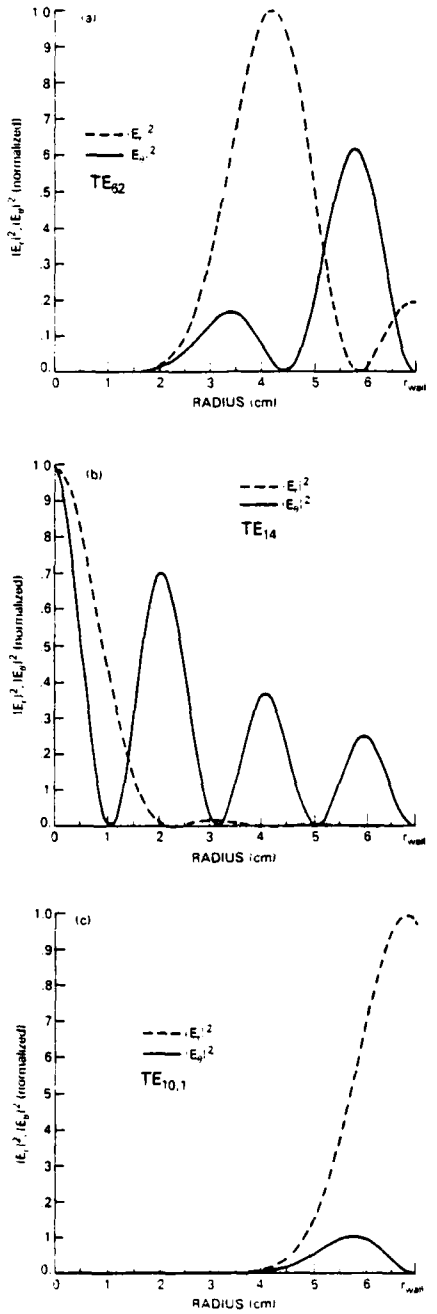

Fig. 5. Predicted microwave power as a function of radius across the experimental output window for (a) the TE_{62} mode, (b) the TE_{14} mode, and (c) the $TE_{10,1}$ mode. Each mode is separately normalized to a peak value of 1.0.

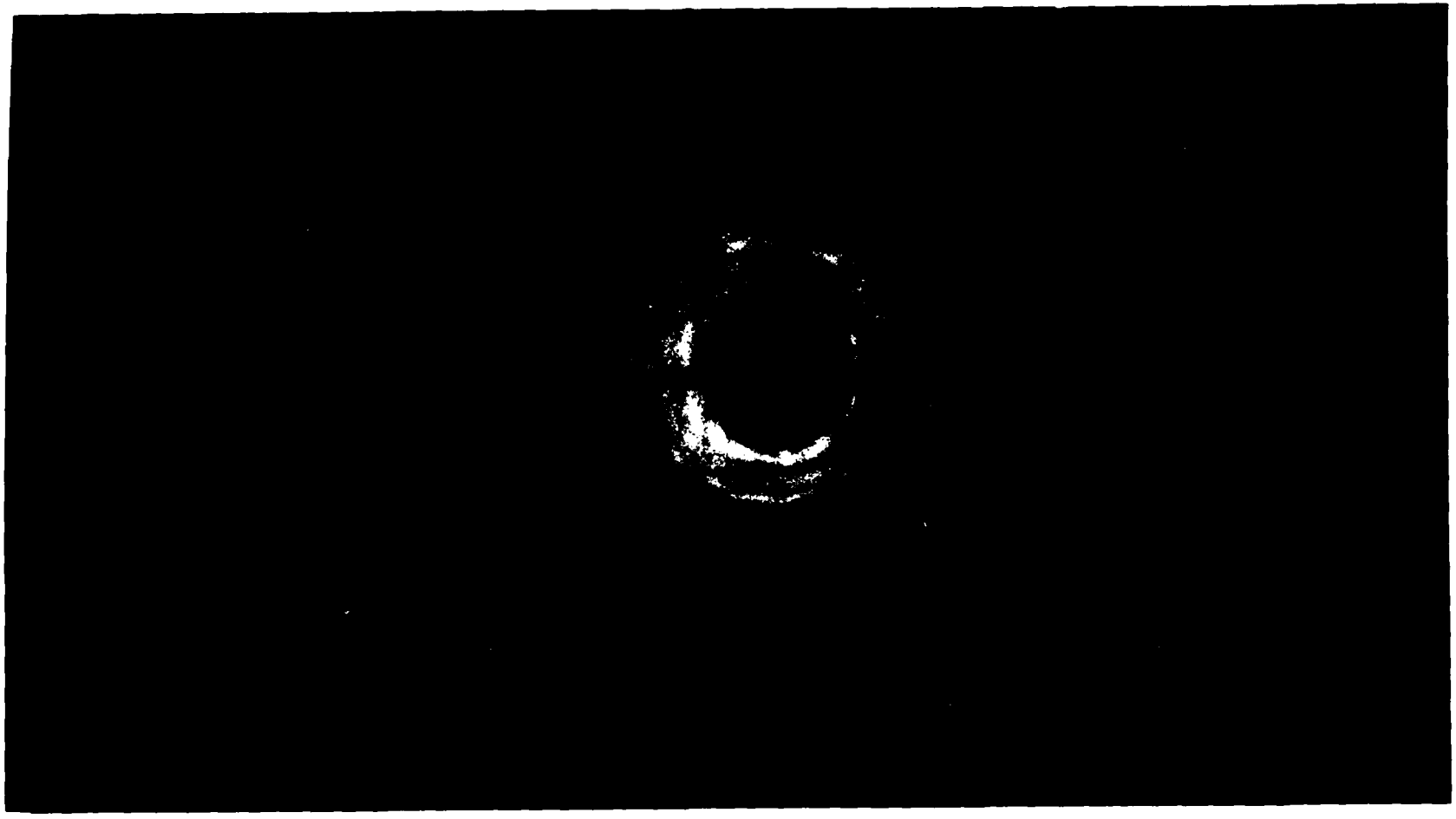

Fig. 6. Open-shutter photograph of gas breakdown across the experimental output window for the parameters of Fig. 4. (The outer halo is a reflection in the walls of the breakdown cell. Vertical and horizontal lines are cm rulings on the window face.)

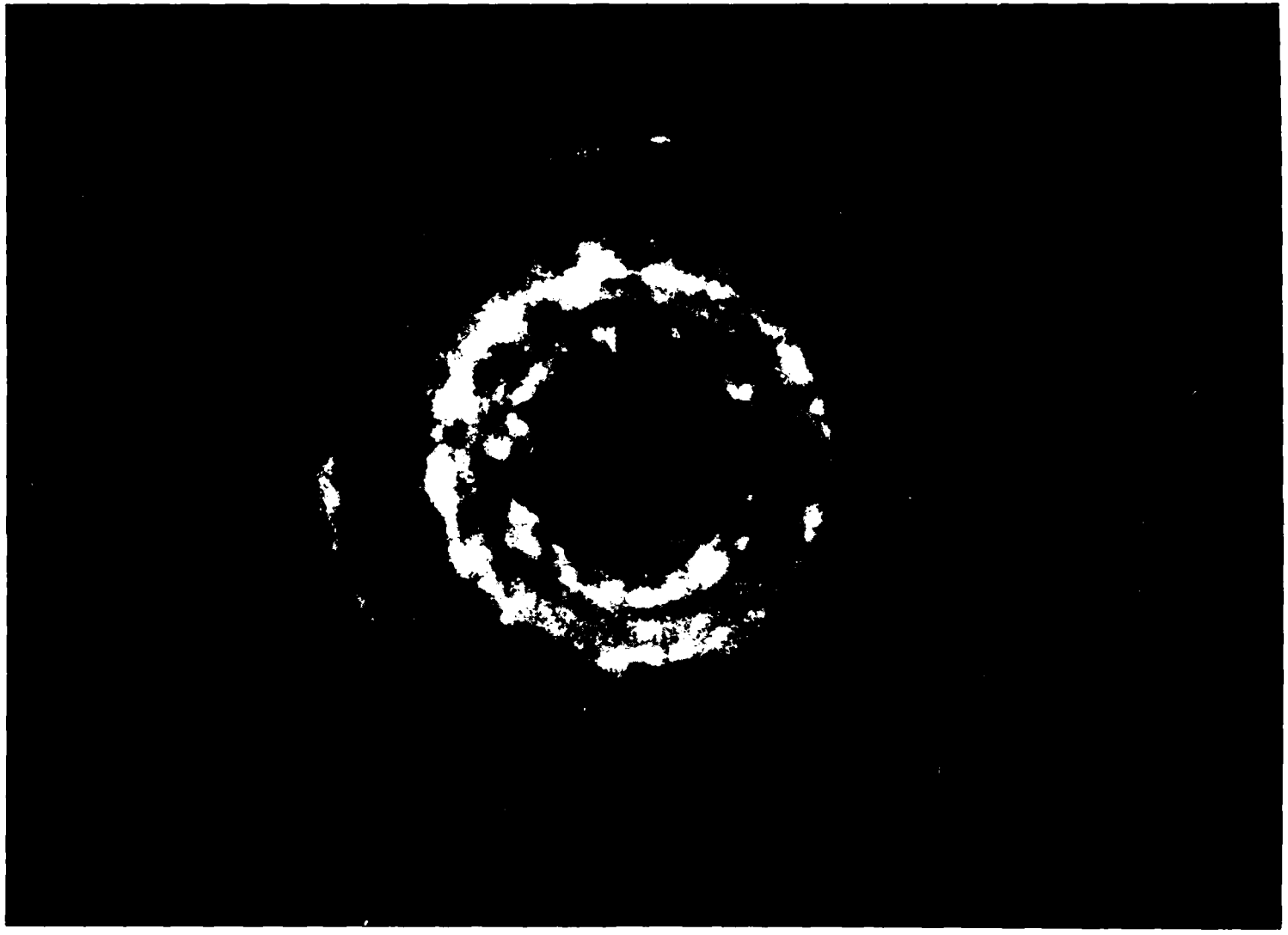

Fig. 7. Open-shutter photograph of gas breakdown across the experimental output window, with the beam radius increased ~10%.

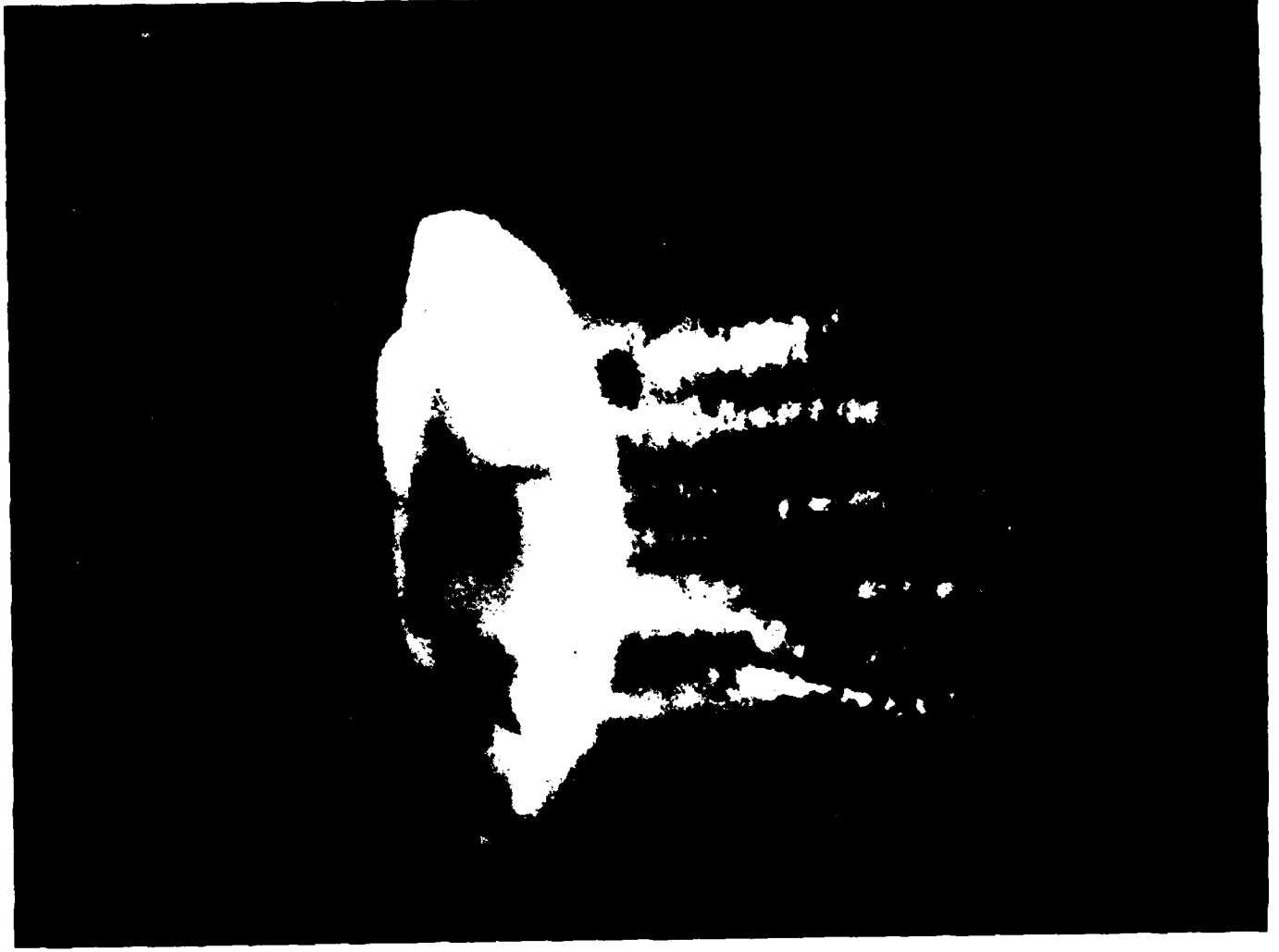

Fig. 8. Side-on photograph of gas breakdown, showing streamers projecting outward from the breakdown at the window face (left) at the azimuthal maxima of a TE_{6n} mode.

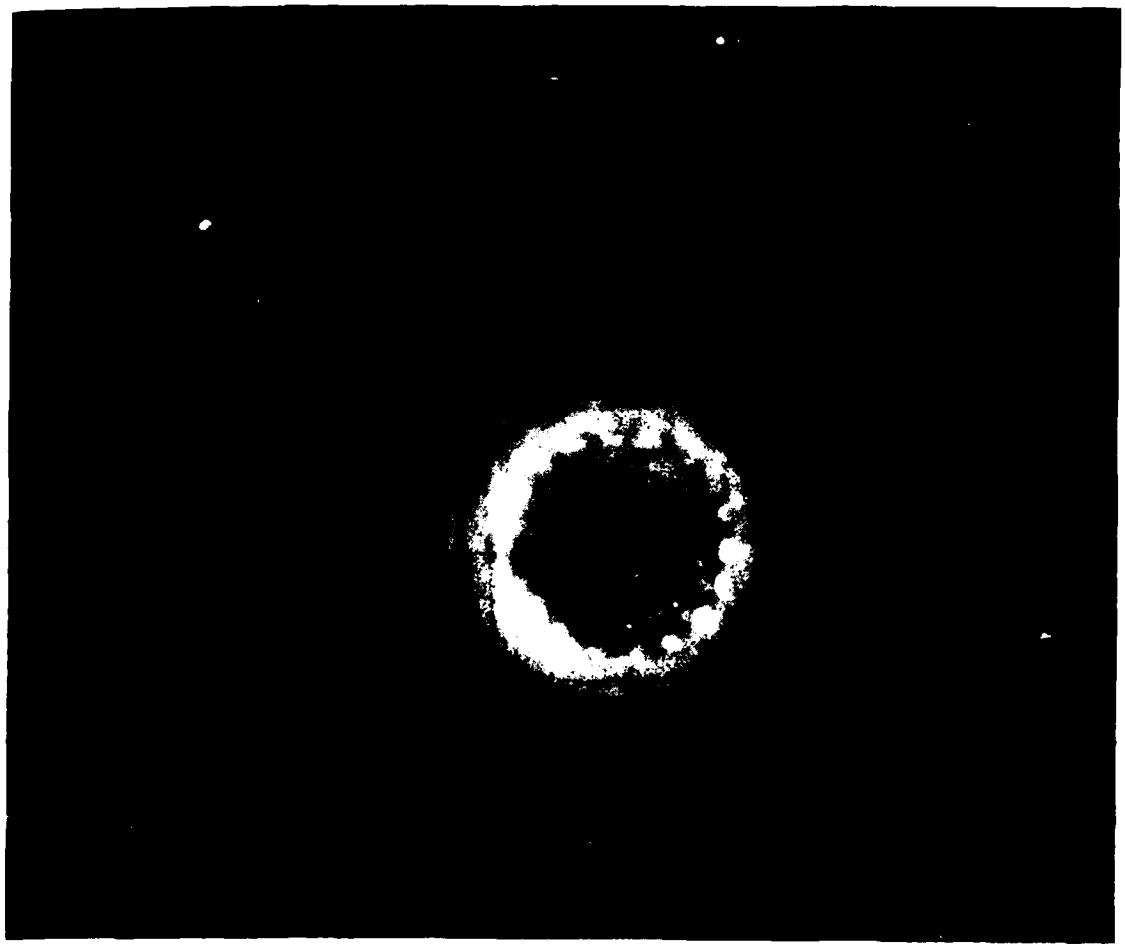

Fig. 9. Open-shutter photograph of gas breakdown across the experimental output window, showing a standing TE_{9n} mode.

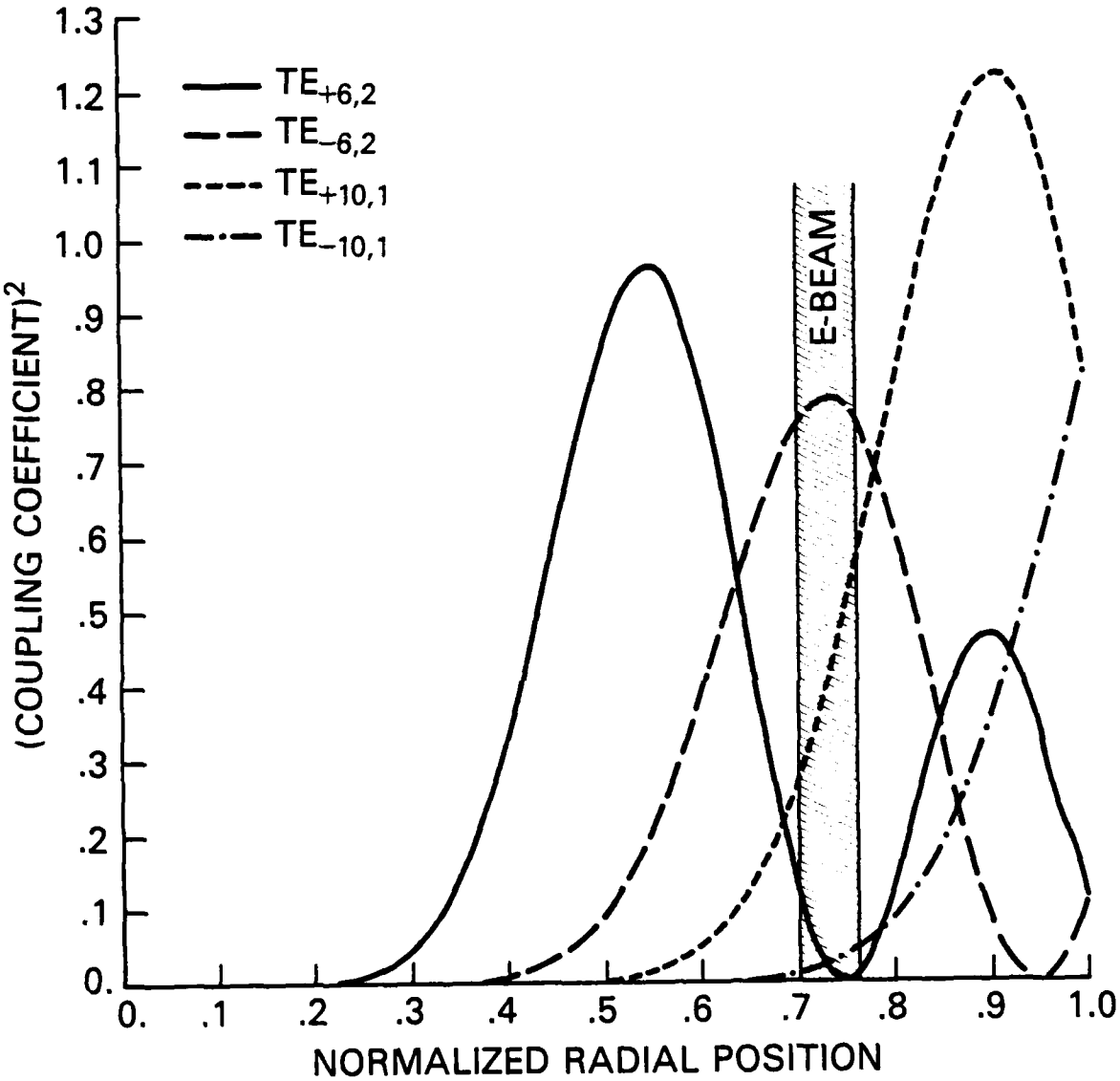

Fig. 10. Plot of the coupling coefficient squared vs normalized cavity radius for $TE_{\pm 6,2}$ and $TE_{\pm 10,1}$ modes. The electron beam position corresponding to the data of Fig. 4 is indicated.

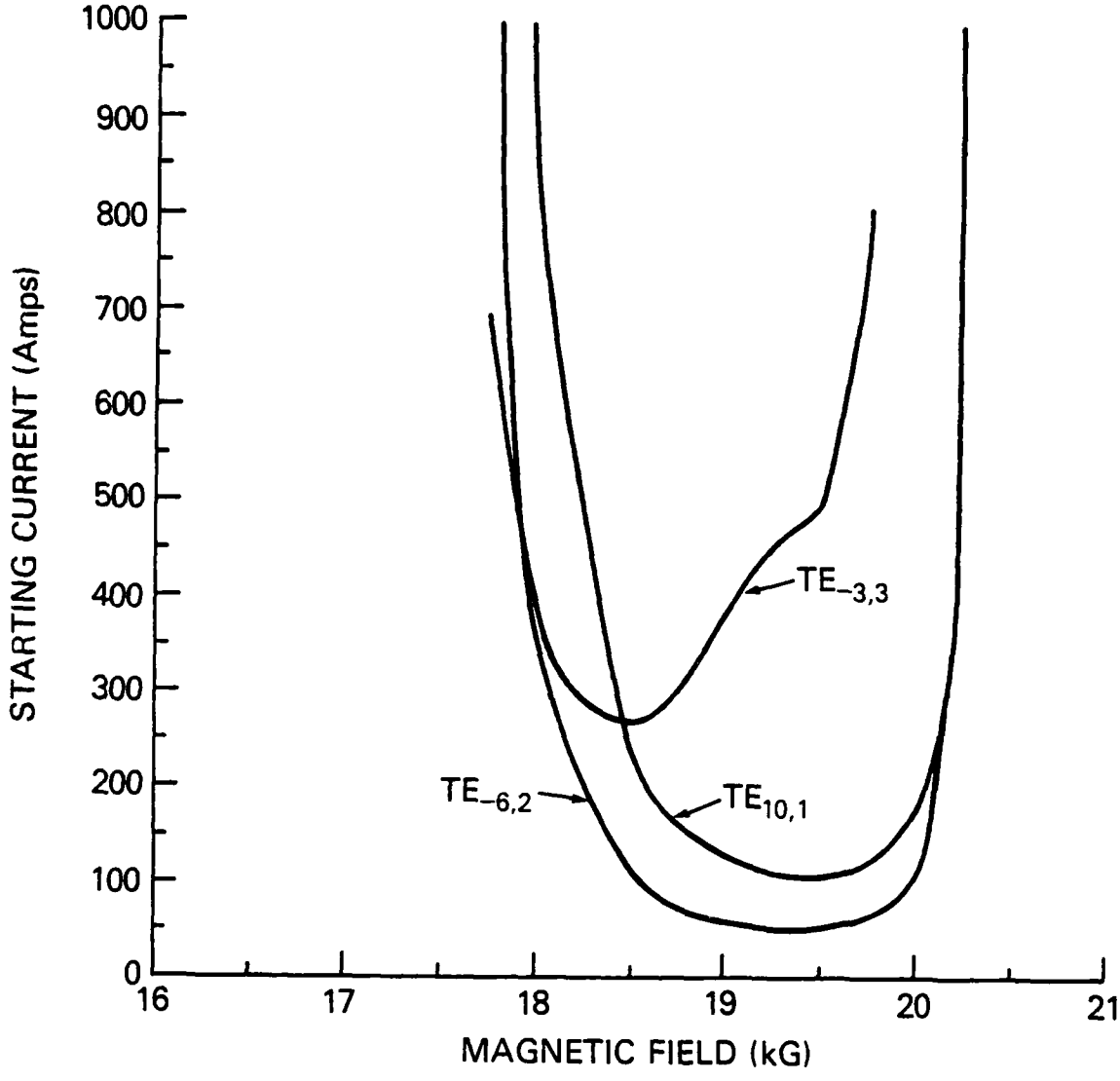

Fig. 11. Plot of the calculated starting current vs cavity magnetic field for a 350 keV electron beam with 1.16 cm radius and α=0.75.

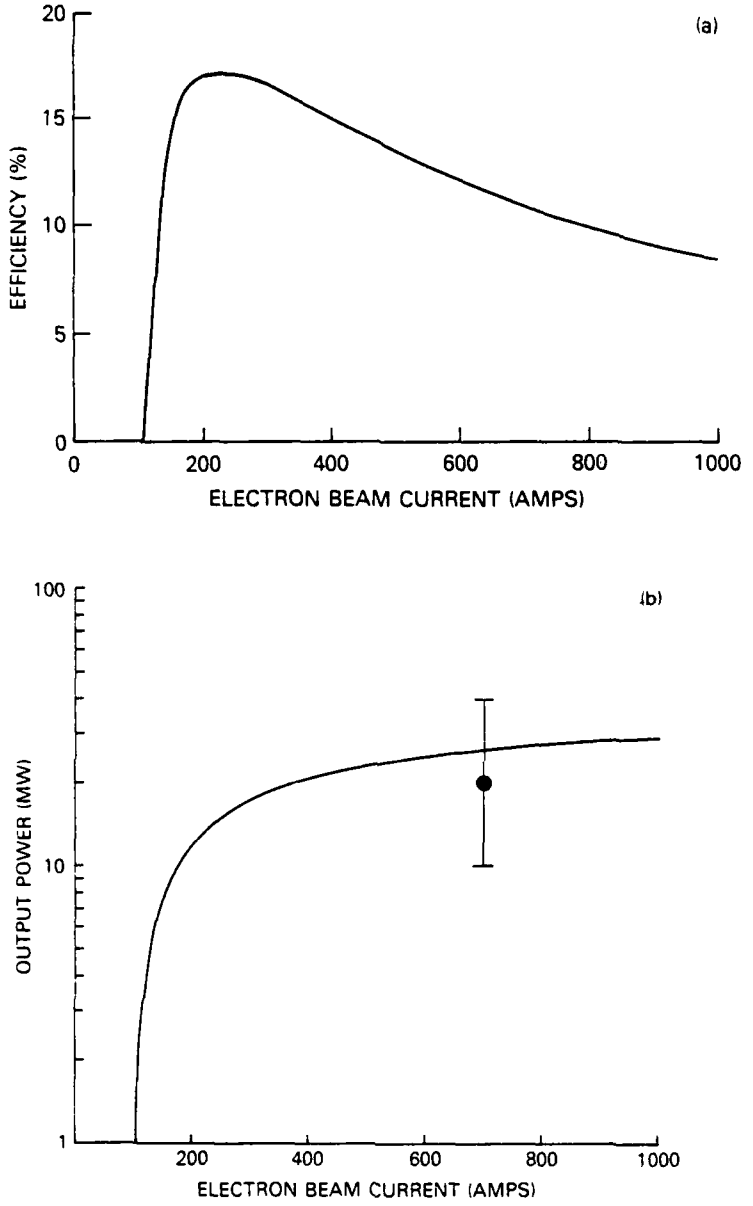

Fig. 12. Plot of (a) theoretical efficiency and (b) theoretical output power vs electron beam current for a $TE_{-6,2}$ gyrotron cavity mode. A 350 keV electron beam with 1.16 cm radius and α=0.75 is assumed. The experimental output power at an electron beam current of 700 A is indicated.

References

†Also at George Mason University, Fairfax, VA 22030.

‡Electrical Engineering Department, University of Maryland, College Park, MD 20742.

¶JAYCOR, Inc., Alexandria, VA 22304.

1. V.A. Flyagin, A.L. Gol'denberg, and G.S. Nusinovich, "Powerful Gyrotrons," in Infrared and Millimeter Waves, edited by K.J. Button (Academic Press, New York, 1984), vol. 11, pp. 179-226.

2. V.L. Granatstein, M. Herndon, P. Sprangle, Y. Carmel, and J.A. Nation, "Gigawatt microwave emission from an intense relativistic electron beam," Plasma Phys., vol. 17, pp. 23-28, 1975.

3. Y. Carmel, K.R. Chu, D. Dialetis, A.W. Fliflet, M.E. Read, K.J. Kim, B. Arfin, and V.L. Granatstein, "Mode competition, suppression, and efficiency enhancement in overmoded gyrotron oscillators," Int. J. Infrared and Millimeter Waves, vol. 3, pp. 645-665, 1982.

4. K. Felch, R. Bier, L. Fox, H. Huey, L. Ives, H. Jory, N. Lopez, J. Manca, J. Shively, and S. Spang, "A 60 GHz, 200 kW cw gyrotron with a pure output mode," Int. J. Electron., vol. 57, pp. 815-820, 1984.

5. N.S. Ginzburg, V.I. Krementsov, M.I. Petelin, P.S. Strelkov, and A.K. Shkvarunets, "Experimental investigation of a high-current relativistic cyclotron maser," Zh. Tekh. Fiz., vol. 49, pp. 378-385, 1979 [Sov. Phys. Tech. Phys., vol. 24, pp. 218-222, 1979].

6. A.N. Didenko, A.G. Zherlitsyn, V.I. Zelentsov, A.S. Sulakshin, G.P. Fomenko, Yu.G. Shtein, and Yu.G. Yushkov, "Generation of gigawatt microwave pulses in the nanosecond range," Fiz. Plazmy, vol. 2, pp. 514-517, 1975 [Sov. J. Plasma Phys., vol. 2, pp. 283-285, 1977].

7. S.N. Voronkov, V.I. Krementsov, P.S. Strelkov, and A.G. Shkvarunets, "Stimulated cyclotron radiation at millimeter wavelengths from high-power relativistic electron beams," Zh. Tekh. Fiz., vol. 52, pp. 106-108, 1982 [Sov. Phys. Tech. Phys. vol. 27, pp. 68-69, 1982].

8. W.B. Herrmannsfeldt, "Electron Trajectory Program," SLAC Report 226, Stanford Linear Accelerator Center, Stanford, CA, 1979.

9. Yu.V. Bykov and A.L. Gol'denberg, "Influence of resonator profile on the maximum power of a cyclotron-resonance maser," Izv. Vyssh. Uchebn. Zaved., Radiofiz., vol. 18, pp. 1066-1067, 1975 [Radiophys. and Quantum Electron., vol. 18, pp. 791-792, 1975].

10. A.W. Fliflet and M.E. Read, "Use of weakly irregular waveguide theory to calculate eigenfrequencies, Q values, and rf field functions for gyrotron oscillators," Int. J. Electron., vol. 51, pp. 475-484, 1981.

11. A.W. Fliflet, "Scaling calculations for the relativistic gyrotron," NRL Memorandum Report 5598 (1985).

12. V.I. Krementsov, P.S. Strelkov, and A.G. Shkvarunets, "Measurement of the parameters of a relativistic high-current electron beam by recording the luminescence of thin dielectric films," Zh. Tekh. Fiz., vol. 50, pp. 2469-2472, 1980 [Sov. Phys. Tech. Phys., vol. 25, pp. 1447-1449, 1980].

13. V.V. Bogdanov, S.N. Voronkov, V.I. Krementsov, P.S. Strelkov, V.Yu. Shafer, and A.G. Shkvarunets, "Measurement of millimeter-range cyclotron radiation induced by a high-current electron beam," Zh. Tekh. Fiz., vol. 53, pp. 106-113, 1983 [Sov. Phys. Tech. Phys., vol. 28, pp. 61-65, 1983].

14. B.C. DeLoach, Jr., "Step-twist-junction waveguide filters," IRE Trans. Microwave Theory Tech., vol. 9, pp. 130-135, 1961.

15. V.L. Bratman, N.S. Ginzburg, G.S. Nusinovich, M.I. Petelin, and P.S. Strelkov, "Relativistic gyrotrons and cyclotron autoresonance masers," Int. J. Electron., vol. 51, pp. 541-567, 1981.

16. A.W. Fliflet, M.E. Read, K.R. Chu, and R. Seeley, "A self-consistent field theory for gyrotron oscillators: application to a low Q gyromonotron," Int. J. Electron., vol. 53, pp. 505-521, 1982.

17. Y.Y. Lau, "Simple macroscopic theory of cyclotron maser instabilities", IEEE Trans. Electron Devices, vol. ED-29, pp. 320-335, 1982.

18. J.M. Finn, A.W. Fliflet, and W.M. Manheimer, "One-dimensional models for relativistic electron beam diode design," Int. J. Electron., to be published.

DISTRIBUTION LIST

Air Force Avionics Laboratory
AFWAL/AADM-1
Wright/Patterson AFB, Ohio 45433
Attn: Walter Friez — 1 copy

Air Force Office of
Scientific Research
Bolling AFB
Washington, D.C. 20332
Attn: H. Schlossberg — 1 copy

Air Force Weapons Lab
Kirkland AFB
Albuquerque, New Mexico 87117
Attn: J. Generosa — 1 copy
C. Clark — 1 copy

Columbia University
520 West 120th Street
Department of Electrical Engineering
New York, N.Y. 10027
Attn: Dr. S.P. Schlesinger — 1 copy

Columbia University
520 West 120th Street
Department of Applied Physics
and Nuclear Engineering
New York, New York 10027
Attn: T.C. Marshall — 1 copy

Cornell University
School of Applied and Engineering Physics
Ithica, New York 14853
Attn: Prof. Hans H. Fleischmann — 1 copy
John Nation — 1 copy

Dartmouth College
18 Wilder, Box 6127
Hanover, New Hampshire 03755
Attn: Dr. John E. Walsh — 1 copy

Department of Energy
Washington, D.C. 20545
Attn: C. Finfgeld/ER-542, GTN — 1 copy
T.V. George/ER-531, GTN — 1 copy
D. Crandall/ER-55, GTN — 1 copy

Defense Advanced Research Project Agency/DEO
1400 Wilson Blvd.
Arlington, Virginia 22209
Attn: Dr. S. Shey — 1 copy

Defense Communications Agency
Washington, D.C. 20305
Attn: Dr. Pravin C. Jain
Assistant for Communications
Technology — 1 copy

Defense Nuclear Agency
Washington, D.C. 20305
Attn: Mr. J. Farber — 1 copy
Maj. J. Benson — 1 copy
Capt. D. Stone — 1 copy
Mr. Lloyd Stossell — 1 copy

Defense Technical Information Center
Cameron Station
5010 Duke Street
Alexandria, Virginia 22314 — 2 copies

Georgia Tech. EES-EOD
Baker Building
Atlanta, Georgia 30332
Attn: Dr. James J. Gallagher — 1 copy

Hanscomb Air Force Base
Stop 21, Massachusetts 01731
Attn: Lt. Rich Nielson/ESD/INK — 1 copy

Hughes Aircraft Co.
Electron Dynamics Division
3100 West Lomita Boulevard
Torrance, California 90509
Attn: J. Christiansen — 1 copy
J.J. Tancredi — 1 copy

KMS Fusion, Inc.
3941 Research Park Dr.
P.O. Box 1567
Ann Arbor, Michigan 48106
Attn: S.B. Segall — 1 copy

Lawrence Livermore National Laboratory
P.O. Box 808
Livermore, California 94550
Attn: Dr. D. Prosnitz — 1 copy
Dr. T.J. Orzechowski — 1 copy
Dr. J. Chase — 1 copy

Los Alamos Scientific Laboratory
P.O. Box 1663, AT5-827
Los Alamos, New Mexico 87545
Attn: Dr. J.C. Goldstein — 1 copy
Dr. T.J.T. Kwan — 1 copy
Dr. L. Thode — 1 copy
Dr. C. Brau — 1 copy

Massachusetts Institute of Technology
Department of Physics
Cambridge, Massachusetts 02139

Attn: Dr. G. Bekefi/36-213	1 copy
Dr. M. Porkolab/NW 36-213	1 copy
Dr. R. Davidson/NW 16-206	1 copy
Dr. A. Bers/NW 38-260	1 copy

Massachusetts Institute of Tech.
167 Albany St., N.W. 16-200
Cambridge, Massachusetts 02139

Attn: Dr. R. Temkin/NW 14-4107	1 copy

Mathematical Sciences Northwest, Inc.
Bellevue, Washington 90004

Attn: Dr. J.M. Slater	1 copy

Mission Research Corp.
1720 Randolph Road, S.E.
Albuquerque, New Mexico 87106

Attn: Dr. Ken Busby	1 copy
Mr. Brendan B. Godfrey	1 copy

Naval Electronic Systems Command
Washington, D.C. 20363

Attn: E. Warden	
Code PDE 106-3113	1 copy

Naval Research Laboratory

Addressee: Attn: Name/Code	
Code 1001 - T. Coffey	1 copy
Code 2628 - TID Distribution	20 copies
Code 4000 - W. Ellis	1 copy
Code 4700 - S. Ossakow	26 copies
Code 4700.1 - A.W. Ali	1 copy
Code 4704 - C. Kapetanakos	1 copy
Code 4740 - Branch Office	25 copies
Code 4740 - W. Black	1 copy
Code 4740 - J. Condon	1 copy
Code 4740 - A. Fliflet	1 copy
Code 4740 - S. Gold	1 copy
Code 4740 - A. Kinkead	1 copy
Code 4740 - W.M. Manheimer	1 copy
Code 4740 - M.E. Read	1 copy
Code 4740 - M. Rhinewine	1 copy
Code 4770 - G. Cooperstein	1 copy
Code 4790 - B. Hui	1 copy
Code 4790 - C.M. Hui	1 copy
Code 4790 - Y.Y. Lau	1 copy
Code 4790 - P. Sprangle	1 copy
Code 5700 - L.A. Cosby	1 copy
Code 6840 - S.Y. Ahn	1 copy
Code 6840 - A. Ganguly	1 copy
Code 6840 - R.K. Parker	1 copy

Code 6840 - N.R. Vanderplaats 1 copy
Code 6850 - L.R. Whicker 1 copy
Code 6875 - R. Wagner 1 copy

Naval Sea Systems Command
Department of the Navy
Washington, D.C. 20362
Attn: Commander George Bates
PMS 405-300 1 copy

Northrop Corporation
Defense Systems Division
600 Hicks Rd.
Rolling Meadows, Illinois 60008
Attn: Dr. Gunter Dohler 1 copy

Oak Ridge National Laboratory
P.O. Box Y
Mail Stop 3
Building 9201-2
Oak Ridge, Tennessee 37830
Attn: Dr. A. England 1 copy
M. Loring 1 copy

Office of Naval Research
800 N. Quincy Street
Arlington, Va. 22217
Attn: Dr. C. Roberson 1 copy
Dr. W. Condell 1 copy
Dr. T. Berlincourt 1 copy

Office of Naval Research
1030 E. Green Street
Pasadena, CA 91106
Attn: Dr. R. Behringer 1 copy

Optical Sciences Center
University of Arizona
Tucson, Arizona 85721
Attn: Dr. Willis E. Lamb, Jr. 1 copy

Pacific Missile Test Center
Code 0141-5
Point Muga, California 93042
Attn: Will E. Chandler 1 copy

Physical Dynamics, Inc.
P.O. Box 10367
Oakland, California 94610
Attn: A. Thomson 1 copy

Physics International
2700 Merced Street
San Leandro, California 94577
Attn: Dr. J. Benford — 1 copy

Princeton Plasma
Plasma Physics Laboratory
James Forrestal Campus
P.O. Box 451
Princeton, New Jersey 08544
Attn: Dr. H. Hsuan — 2 copies

Quantum Institute
University of California
Santa Barbara, California 93106
Attn: Dr. L. Elias — 1 copy

Raytheon Company
Microwave Power Tube Division
Foundry Avenue
Waltham, Massachusetts 02154
Attn: N. Dionne — 1 copy

Sandia National Laboratories
ORG. 1231, P.O. Box 5800
Albuquerque, New Mexico 87185
Attn: Dr. Thomas P. Wright — 1 copy
Mr. J.E. Powell — 1 copy
Dr. J. Hoffman — 1 copy
Dr. W.P. Ballard — 1 copy

Science Applications, Inc.
1710 Goodridge Dr.
McLean, Virginia 22102
Attn: Adam Drobot — 1 copy

Stanford University
High Energy Physics Laboratory
Stanford, California 94305
Attn: Dr. T.I. Smith — 1 copy

TRW, Inc.
Space and Technology Group
Suite 2600
1000 Wilson Boulevard
Arlington, VA 22209
Attn: Dr. Neil C. Schoen — 1 copy

TRW, Inc.
Redondo Beach, California 90278
Attn: Dr. H. Boehmer — 1 copy

University of California
Physics Department
Irvine, California 92717
Attn: Dr. G. Benford — 1 copy
Dr. N. Rostoker — 1 copy

University of California
Department of Physics
Los Angeles, CA 90024
Attn: Dr. A.T. Lin — 1 copy
Dr. N. Luhmann — 1 copy
Dr. D. McDermott — 1 copy

University of Maryland
Department of Electrical Engineering
College Park, Maryland 20742
Attn: Dr. V. L. Granatstein — 1 copy

University of Maryland
Laboratory for Plasma and Fusion
Energy Studies
College Park, Maryland 20742
Attn: Dr. Jhan Varyan Hellman — 1 copy
Dr. John McAdoo — 1 copy

University of Tennessee
Dept. of Electrical Engr.
Knoxville, Tennessee 37916
Attn: Dr. I. Alexeff — 1 copy

University of New Mexico
Department of Physics and Astronomy
800 Yale Blvd, N.E.
Albuquerque, New Mexico 87131
Attn: Dr. Gerald T. Moore — 1 copy

University of Utah
Deparment of Electrical Engineering
3053 Merrill Engineering Bldg.
Salt Lake City, Utah 84112
Attn: Dr. Larry Barnett — 1 copy
Dr. J. Mark Baird — 1 copy

Varian Associates
611 Hansen Way
Palo Alto, California 94303
Attn: Dr. H. Jory — 1 copy
Dr. David Stone — 1 copy
Dr. Kevin Felch — 1 copy

Westinghouse Electric Corporation
1310 Beulah Road
Pittsburgh, Pennsylvania 15235
Attn: Dr. Anthony Lee — 1 copy

Yale University
Applied Physics
Madison Lab
P.O. Box 2159
Yale Station
New Haven, Connecticut 06520

Attn: Dr. J. Hirshfield	1 copy
Dr. N. Ebrahim	1 copy
Dr. I. Bernstein	1 copy

Director of Research U.S. Naval Academy Annapolis, MD 21402	2 copies
Code 1220	1 copy